Hindawi Publishing Corporation
International Journal of Photoenergy
Volume 2014, Article ID 952528, 8 pages
http://dx.doi.org/10.1155/2014/952528

Research Article

Investigation of Thermal Instability of Additive-Based High-Efficiency Organic Photovoltaics

En-Ping Yao, Yi-Jhe Tsai, and Wei-Chou Hsu

Institute of Microelectronics, Department of Electrical Engineering and Advanced Optoelectronic Technology Center, National Cheng Kung University, Tainan 70101, Taiwan

Correspondence should be addressed to Wei-Chou Hsu; wchsu@eembox.ncku.edu.tw

Received 15 April 2014; Revised 15 June 2014; Accepted 18 July 2014; Published 10 August 2014

Academic Editor: Harald Hoppe

Most photovoltaics operate at high temperature under sunlight. In this work, the thermal instability of diiodooctane-based high-efficiency bulk heterojunction (BHJ) organic photovoltaics (OPVs) is studied. The BHJ layers were heated to various temperatures to investigate the changes in their physical properties using atomic force microscopy phase images. The mobilities of the carriers were characterized at various temperatures using the space-charge-limited current method, and the carrier lifetime was calculated by applying impedance spectroscopy to the simulated equivalent circuit of the OPV devices.

1. Introduction

Organic photovoltaics (OPVs) have received interest due to their simple fabrication and potential for large-area devices [1]. OPVs commonly have a bulk heterojunction (BHJ) [2–7] structure, where *p*-type (donor) and *n*-type (acceptor) materials are mixed to increase the area of the donor/acceptor interface to effectively extract electrons and holes from excitons. The efficiencies of single and tandem OPVs have reached around 9% [8] and 10.2% [9].

OPVs with a BHJ structure can be fabricated using a solution process. The morphology of the active layer determines light soaking performance. The carrier extraction from excitons to the electrodes is difficult to control. To form a BHJ layer with a favorable morphology, methods such as thermal annealing, solvent annealing, and additive addition have been applied to modify the crystallization of materials to improve the interaction and interpenetration between holes and electrons. Recently, additives such as diiodooctane (DIO) [10, 11], 1,8-octanedithiol (OT) [12], 1-chloronaphthalene (CN) [13], and nitrobenzene (NB) [14] have been introduced to change the morphology of the BHJ layer. These changes are due to the difference in volatility between the main solvent and the additive and the difference in solubility between the donor and acceptor materials and that of the main solvent and the additive. High-efficiency OPV single cells have been derived [8] using a light-harvesting layer, thieno[3,4-b]thiophene/benzodithiophene (PTB7): [6,6]-phenyl C71-butyric acid methyl ester ($PC_{71}BM$), blended with 3% DIO, reaching a power conversion efficiency (PCE) of 9.214%.

Although high-performance devices have been obtained by controlling the morphology of the BHJ layer, to prevent the PCE from degrading, the arrangement of the donor and acceptor materials should be stable under working conditions. However, most photovoltaics are exposed to direct sunlight, and thus they harvest not only light but also radiant heat. In OPVs, heat determines the crystallization of the donor and acceptor materials and affects the morphology of the BHJ layer. Hence, the thermal stability of the donor and acceptor materials in the BHJ layer is very critical to the performance of OPV devices exposed to sunlight. The present study investigates the thermal stability of high-efficiency OPV devices based on poly[(4,8-bis-(2-ethylhexyloxy)-benzo[1,2-b;4,5-b′]dithiophene)-2,6-diyl-alt-(4-(2-ethyl-hexanoyl)-thieno[3,4-b]thiopene)-2,6-diyl] (PBDTTT-C): $PC_{71}BM$ BHJ blended with 3% DIO in dichlorobenzene. The effect of heat on the morphological and electrical characteristics of DIO-modified BHJ is investigated.

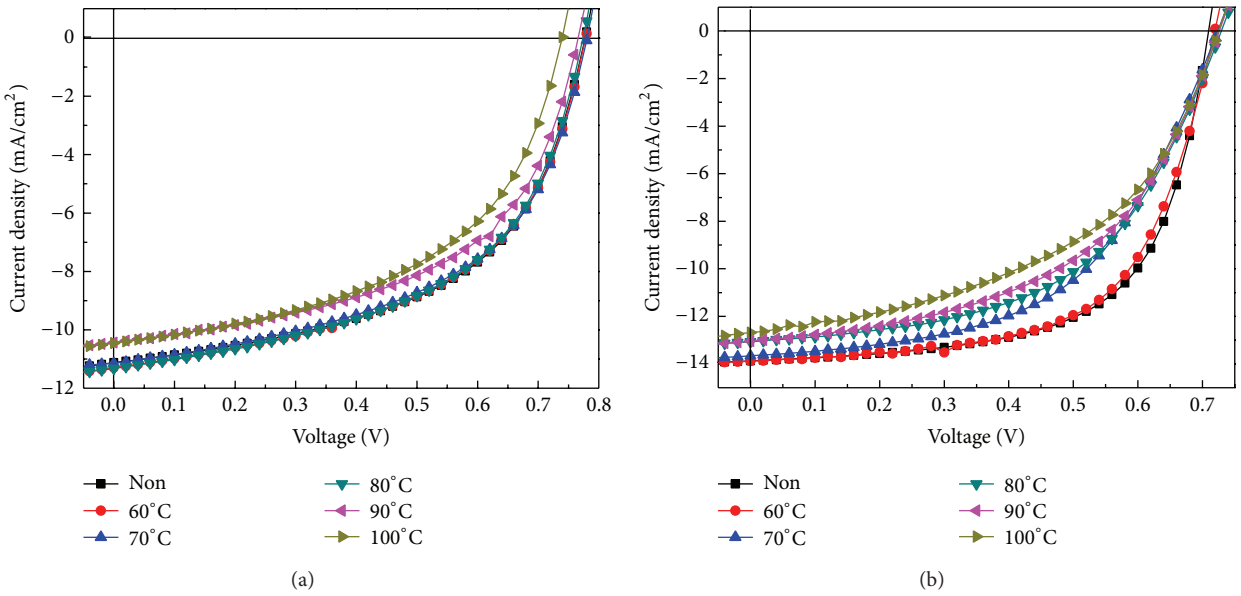

Figure 1: The *J-V* curves of the OPV devices with the PBDTTT-C:$PC_{71}BM$ layers (a) without and (b) with DIO heated under different temperatures for 5 minutes.

Table 1: The *J-V* characteristics the OPV devices with the PBDTTT-C:$PC_{71}BM$ layers heated under different temperatures for 5 minutes.

		V_{oc} (V)	J_{sc} (mA/cm^2)	FF (%)	PCE (%) (max.)	PCE (%) (min./avg.)
Without DIO	Non	0.781	10.86	54.18	4.6	4.38/4.46
	60°C	0.778	11.12	53.55	4.63	4.39/4.57
	70°C	0.778	11.3	52.36	4.6	4.51/4.53
	80°C	0.781	11.14	52.37	4.56	4.32/4.36
	90°C	0.774	11.33	52.32	4.59	4.35/4.4
	100°C	0.767	10.68	53.71	4.4	4.2/4.32
With 3% DIO	Non	0.71	13.87	63.06	6.21	6.09/6.14
	60°C	0.719	13.88	61.16	6.11	6.03/6.07
	70°C	0.724	13.66	52.99	5.24	4.89/5.05
	80°C	0.726	13.07	51.94	4.93	4.83/4.9
	90°C	0.726	13.04	50.95	4.83	4.71/4.77
	100°C	0.725	12.68	48.24	4.43	4.13/4.26

2. Experimental Details

PBDTTT-C:$PC_{71}BM$-based OPVs were fabricated on indium tin oxide- (ITO-) coated glass substrates. The substrates were cleaned with acetone, isopropanol, and deionized water in an ultrasonic cleaner. Before poly(3,4-ethylenedioxythiophene)-poly(styrenesulfonate) (PEDOT:PSS) was coated onto ITO, the substrates were treated with UV zone for 15 min. After a ~30 nm thick layer of PEDOT:PSS was deposited, the film was annealed for 15 min at 120°C. Then, a ~90 nm thick layer of PBDTTT-C:$PC_{71}BM$ was spin-coated on the PEDOT:PSS. The concentration of the PBDTTT-C:$PC_{71}BM$ (1 : 1.5) blend solution for spin-coating was 10 mg/mL (polymer/solvent). 1,2-Dichlorobenzene (DCB) was used as the solvent. DIO was added into the solution (at 3%) to DCB prior to the spin-coating process. Calcium (Ca) and aluminum (Al) layers were deposited on PBDTTT-C:$PC_{71}BM$ in a thermal evaporator with thicknesses of 20 and 100 nm, respectively. The device, with a structure of ITO/PEDOT:PSS/PBDTTT-C:$PC_{71}BM$/Ca/Al, had an area of 0.1 cm^2.

The current density-voltage (*J-V*) characteristics of the OPV devices were measured using a Keithley 2400 source measure unit under AM 1.5 G illumination at 100 mW/cm^2 with a Newport Thermal Oriel 91192 1000-W solar simulator. The external quantum efficiency (EQE) values of the devices were derived using a halogen-tungsten lamp, a monochromator, an optical chopper, and a lock-in amplifier. The photon flux was calibrated using a silicon photodiode.

3. Results and Discussion

3.1. J-V Characteristics. The PBDTTT-C:$PC_{71}BM$ films without DIO were heated to temperatures of 60 to 100°C, respectively, for 5 min on a hot plate. The *J-V* curves of the devices

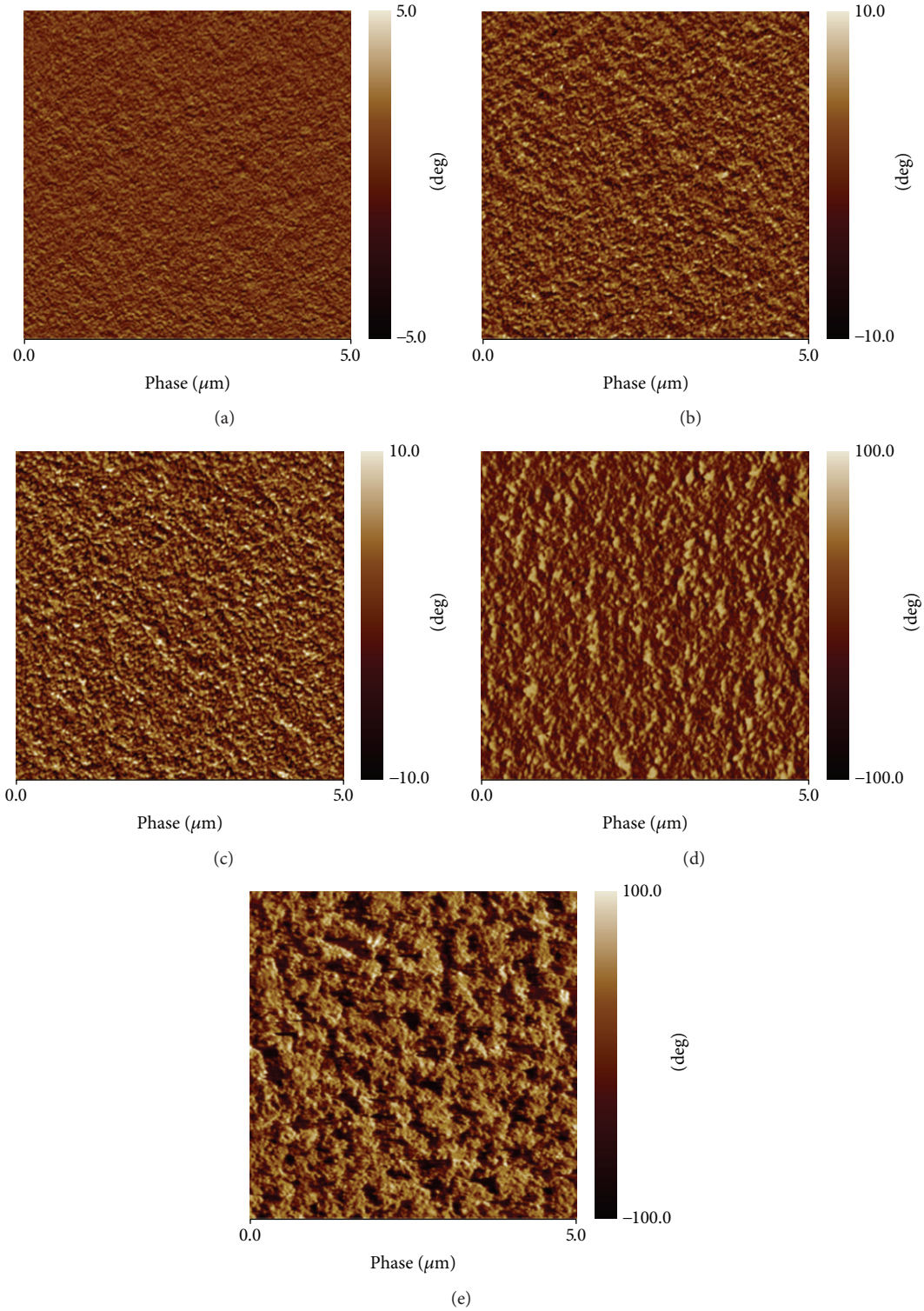

FIGURE 2: The AFM phase images of the PBDTTT-C:$PC_{71}BM$ films with 3% DIO heated under (a) room temperature, (b) 70°C, (c) 80°C, (d) 90°C, and (e) 100°C for 5 minutes.

for various temperatures are shown in Figure 1(a) and the optoelectronic properties are shown in Table 1. As shown, there is little difference in performance for temperatures up to 90°C. In contrast, the device performance drops slightly at a temperature of 100°C, indicating that the interaction between PBDTTT-C and $PC_{71}BM$ in the PBDTTT-C:$PC_{71}BM$ film without DIO begins to vary at 100°C. The morphology of BHJ films without DIO should thus be quite stable below 100°C. With 3% DIO in the PBDTTT-C:$PC_{71}BM$ films, the more favorable morphology would be obtained leading to

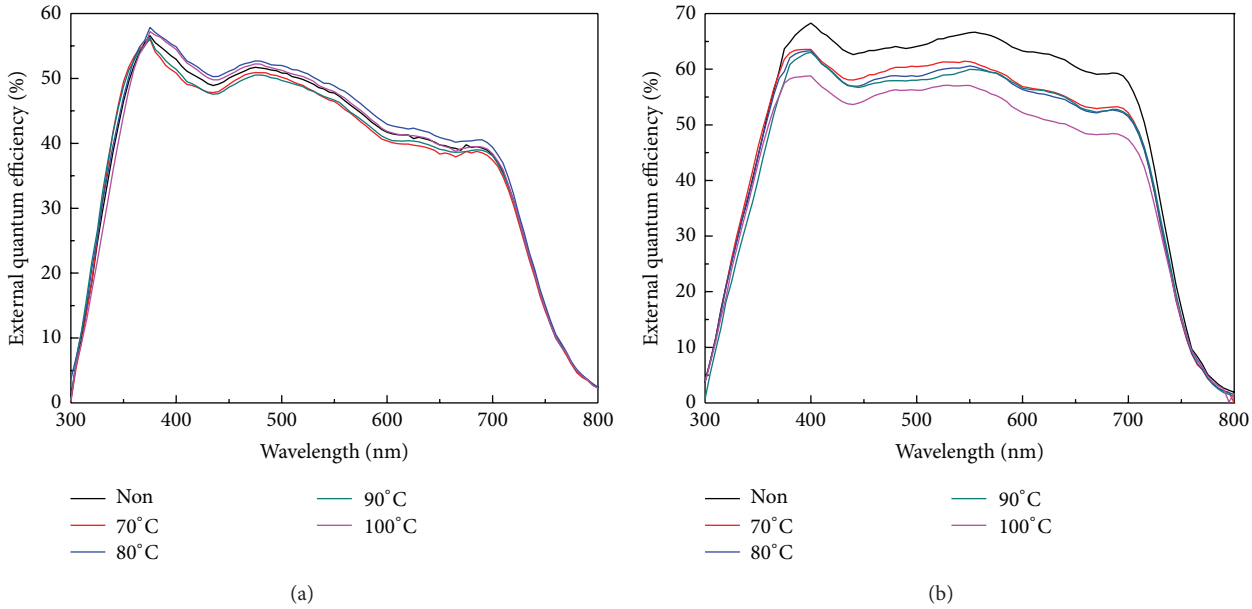

Figure 3: The EQE spectra of the OPV devices with the PBDTTT-C:$PC_{71}BM$ layers (a) without DIO and (b) with 3% DIO heated under different temperatures for 5 minutes.

better performance, and the thermal stability of the BHJ films should be more important. Figure 1(b) shows the *J-V* curves of the OPV devices with PBDTTT-C:$PC_{71}BM$ film with 3% DIO heated to 60 to 100°C, respectively, for 5 min. The optoelectronic properties are listed in Table 1 with 10 devices for each condition. There is nearly no physical difference between the PBDTTT-C:$PC_{71}BM$ film without heating and that heated at 60°C according to the similar *J-V* characteristics. However, the device performance drops significantly for temperatures of 70°C and higher. The open-circuit voltage (V_{oc}) increases slightly and the short-circuit current density (J_{sc}) slightly decreases with increasing temperature. The fill factor (FF) decays dramatically with temperature, dominating the degradation of the PCE. Consequently, although the *J-V* characteristics of the PBDTTT-C:$PC_{71}BM$-based OPV device with DIO are better than those of the device without DIO, the thermal stability of the former is much worse than that of the latter.

3.2. AFM Phase Images. The heating temperatures applied to the films are not high enough to break the chains of PBDTTT-C and burn $PC_{71}BM$, and thus the degradation of the *J-V* characteristics must be attributed to the variation of the interaction between the polymer and $PC_{71}BM$ in the BHJ layer, which correlates to the morphology of the films. Figure 2 shows the atomic force microscopy (AFM) phase images of the PBDTTT-C:$PC_{71}BM$ film without thermal treatment and those heated to 70, 80, 90, and 100°C, respectively, for 5 min. As shown, the phase variation range is large (from ±5° to ±10°) for temperatures of 70 and 80°C, becoming even larger (±100°) at 90 and 100°C. Moreover, the phase separation becomes increasingly obvious with increasing temperature due to the morphological difference between $PC_{71}BM$ clusters and PBDTTT-C chains leading to completely different interactions between the two materials at different temperatures. The more obvious the phase separation, the worse the performance. This is especially true for the device heated to 100°C, whose phase image is extremely different from those of the others.

3.3. EQE and SCLC. The morphology directly affects the carrier penetration in the BHJ layer and thus determines the current collected at the electrodes. Figure 3 shows the EQE values of the devices with the PBDTTT-C:$PC_{71}BM$ layer without and with 3% DIO without thermal treatment and those heated to 70, 80, 90, and 100°C, respectively, for 5 min. The films without DIO under different heating temperatures show nearly no difference on the EQE spectra corresponding to the stable result of the *J-V* characteristics mentioned above. To the films with 3% DIO, the EQE decreases with increasing temperature; however, there is no obvious variation in the shape of the curves, which implies that the heating process does not change the original characteristics of the materials in the BHJ films but instead affects the arrangement of the polymer chains and $PC_{71}BM$ molecules. The EQE curves of the devices heated to 70, 80, and 90°C are similar, as with *J-V* characteristics. With heating to 100°C, the EQE drops by about 20%, accompanied by a significant drop in *J-V* performance and entirely different phase images compared to those of the other devices. The variation on the EQE value is partially determined by the absorption issue of the PBDTTT-C:$PC_{71}BM$ layer. Figure 4 shows the absorption spectra of the PBDTTT-C:$PC_{71}BM$ films without thermal treatment and those heated to 70, 80, 90, and 100°C, respectively, for 5 min. As shown, the absorption intensity of the PBDTTT-C:$PC_{71}BM$ film decreases slightly with the increasing of the

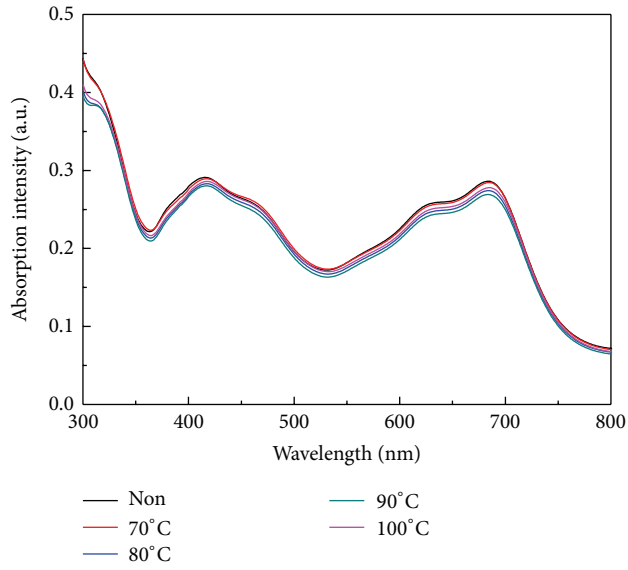

FIGURE 4: Absorption spectra of PBDTTT-C:PC_{71}BM blend films heated under different temperatures for 5 minutes.

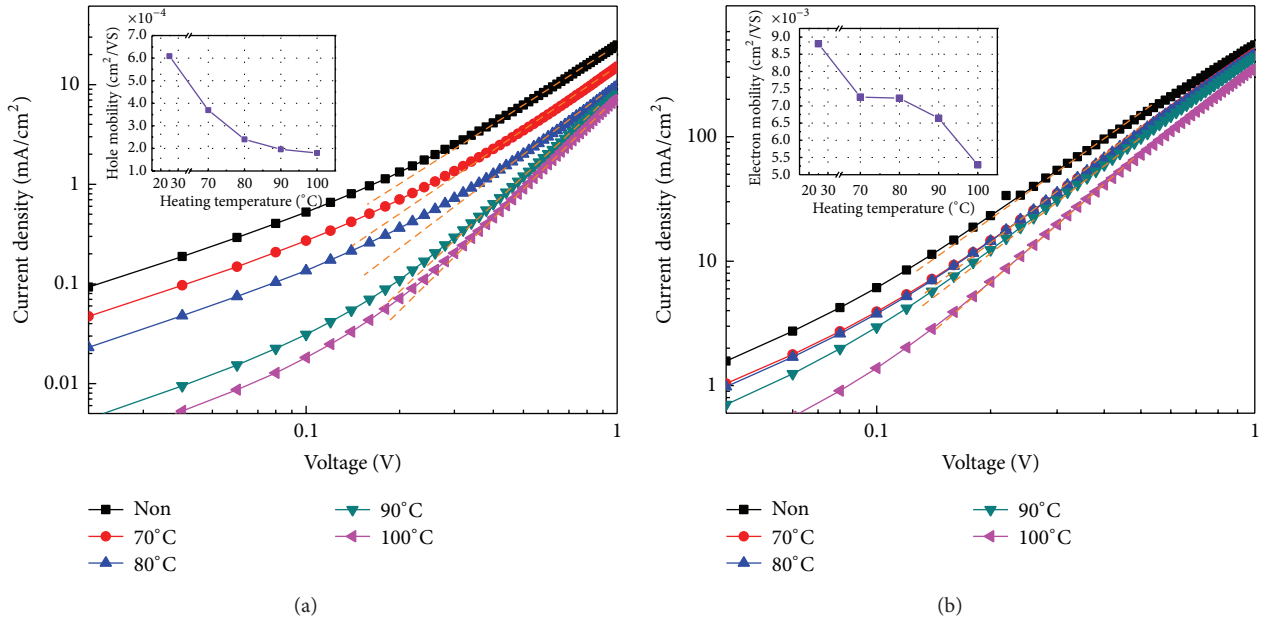

FIGURE 5: The dark *J-V* curves on log-log plots of the (a) hole-only and (b) electron-only OPV devices with the PBDTTT-C:PC_{71}BM layers with 3% DIO heated under different temperatures for 5 minutes.

heating temperature, which indicates that the morphological variation on the bulk heterojunction layer from the heating process affects the absorption property of the film, but hardly. Therefore, the result from the absorption spectra is still insufficient to elucidate the significant drop on the EQE data. However, the EQE performance is also related to the carrier penetration, which corresponds to the carrier mobility. The hole and electron mobilities in the PBDTTT-C:PC_{71}BM layer of devices heated to various temperatures were extracted using the space-charge-limited current (SCLC) method [15, 16]. The structures of hole-only and electron-only devices are ITO/PEDOT:PSS/PBDTTT-C:PC_{71}BM/molybdenum trioxide (MoO_3)/Al and Al/PBDTTT-C:PC_{71}BM/Ca/Al, respectively. The *J-V* curves of devices heated to various temperatures are shown in Figure 5. According to the *J-V* characteristics of the hole-only and electron-only devices, the steady-state current density J_{SCLC} is theoretically a function of the applied voltage V, the film thickness d, the relative

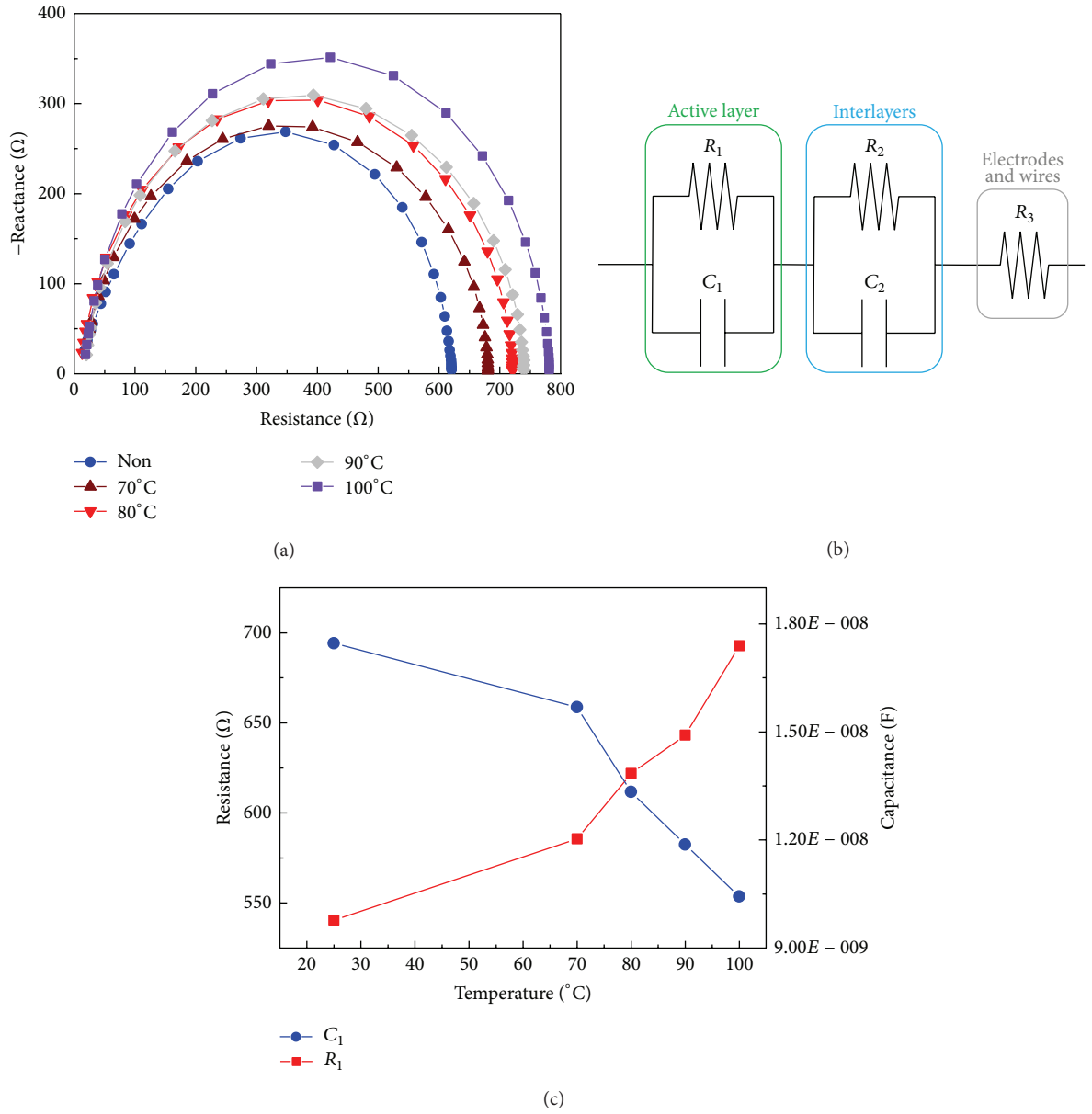

Figure 6: The (a) Cole-Cole plot, (b) equivalent circuit, and (c) simulated data of R_1 and C_1 of the OPV devices with the PBDTTT-C:$PC_{71}BM$ layers heated under different temperatures for 5 minutes.

dielectric constant ε_r, the vacuum permeability ε_0, and the steady-state charge-carrier mobility μ_{SCLC}:

$$J_{SCLC} = \frac{9}{8}\mu_{SCLC}\varepsilon_r\varepsilon_0\frac{V^2}{d^3}. \quad (1)$$

The relative dielectric constant was assumed to be 3, and the extracted mobilities are reported in the inset of Figures 5(a) and 5(b), respectively. As the PBDTTT-C:$PC_{71}BM$ film was heated from 70 to 100°C, the hole mobility and electron mobility of the hole-only and electron-only devices dropped gradually, which indicates that the electron and hole mobilities are getting worse simultaneously with the increasing temperature. However, the hole mobility degrades much more severely than does electron mobility, which indicates that the morphology change of $PC_{71}BM$ clusters caused by heating not only reduces the transmission of electrons to the cathode on the acceptor material ($PC_{71}BM$), but also breaks the paths for the penetration of holes to the anode on the donor material (P3HT).

3.4. Impedance Analysis. Morphology also affects the donor/acceptor interface and thus determines the efficiency of the electron and hole extraction from excitons. Therefore, the PBDTTT-C:$PC_{71}BM$ films heated to different temperatures were analyzed using impedance spectroscopy. The impedance spectra, also called Cole-Cole plots, of the devices are shown

Table 2: The simulated data of R_1 and C_1 by applying the Cole-Cole plot into equivalent circuit.

	R_1 (Ω)	C_1 (F)	τ_{avg} (second)	PCE (%)
Non	540.48	$1.7463E-08$	$9.4384E-06$	6.21
70°C	585.65	$1.5688E-08$	$9.1877E-06$	5.24
80°C	621.86	$1.3334E-08$	$8.2919E-06$	4.93
90°C	641.35	$1.1874E-08$	$7.6154E-06$	4.83
100°C	692.81	$1.0436E-08$	$7.2302E-06$	4.43

in Figure 6(a), and a simple equivalent circuit model of the OPV device is shown in Figure 6(b), where the shunt pair with R_1 and C_1 corresponds to the resistance and capacitance of active layer, the shunt pair with R_2 and C_2 corresponds to the resistance and capacitance of the interface between PEDOT:PSS/PBDTTT-C:PC_{71}BM and PBDTTT-C:PC_{71}BM/Ca, and R_3 corresponds to the resistance of the electrodes and wires connected for measurement. In Figure 6(a), the radius of the Cole-Cole plot increases with temperature, which implies that the resistance of the whole device increases. The elements in each part of the device were simulated by applying the Cole-Cole plot to the equivalent circuit model, since the morphology of active layer is affected by heat. The R_1 and C_1 values are shown in Figure 6(c) and listed in Table 2. The thickness of the active layer remains mostly unchanged at around 90 nm before and after the heating process, and thus the increase of R_1 with temperature indicates that the penetration of carriers in the BHJ layer degrades, which is consistent with previous results. C_1 drops gradually with increasing temperature, indicating that the effective dielectric constant of the PBDTTT-C:PC_{71}BM layer decreases. In fact, the interaction between PBDTTT-C chains and PC_{71}BM molecules is still not clear enough. Nevertheless, the carrier transition time [17], also called the average carrier lifetime, in the BHJ layer can be calculated as

$$\tau_{avg} = R \times C, \tag{2}$$

where τ_{avg} is the average carrier lifetime, R is the resistance, and C is the capacitance. The R_1 and C_1 values of each device were substituted into (2) to obtain the average carrier lifetime. The results are listed in Table 2. The data indicate that the average carrier lifetime decreases with increasing temperature, which means that the holes and electrons are more likely to recombine in the BHJ layer at higher temperature. Therefore, the average carrier lifetime directly corresponds to the performance of the OPV devices, where shorter lifetimes lead to lower PCE values, as shown in Table 2. These simulations prove that the electrical interaction between PBDTTT-C chains and PC_{70}BM molecules in the BHJ layer becomes unfavorable for OPV devices at temperatures over 70°C.

4. Conclusion

In this work, the effect of temperature on the performance of DIO-blended high-efficiency BHJ OPV devices was investigated. An unfavorable morphology of the BHJ layer was observed in AFM phase images after heating to over 70°C. The morphology obtained at high temperature not only degraded the EQE characteristics of the BHJ layer but also diminished the carrier penetration, which degraded the performance of the OPV devices. The average carrier lifetimes in the BHJ layer, derived from impedance spectra, shortened with increasing temperature, decreasing the PCE. The thermal stability of OPV devices with DIO is thus a critical issue.

Conflict of Interests

The authors declare that there is no conflict of interests regarding the publication of this paper.

Acknowledgment

This work was supported by the National Science Council of the Republic of China, Taiwan, under Grants NSC 100-2221-E-006-041-MY3 and NSC 100-2221-E-006-039-MY3.

References

[1] L. Blankenburg, K. Schultheis, H. Schache, S. Sensfuss, and M. Schrödner, "Reel-to-reel wet coating as an efficient up-scaling technique for the production of bulk-heterojunction polymer solar cells," *Solar Energy Materials and Solar Cells*, vol. 93, no. 4, pp. 476–483, 2009.

[2] G. Li, V. Shrotriya, J. Huang et al., "High-efficiency solution processable polymer photovoltaic cells by self-organization of polymer blends," *Nature Materials*, vol. 4, no. 11, pp. 864–868, 2005.

[3] W. Ma, C. Yang, X. Gong, K. Lee, and A. J. Heeger, "Thermally stable, efficient polymer solar cells with nanoscale control of the interpenetrating network morphology," *Advanced Functional Materials*, vol. 15, no. 10, pp. 1617–1622, 2005.

[4] G. J. Zhao, Y. J. He, and Y. Li, "6.5% efficiency of polymer solar cells based on poly(3-hexylthiophene) and indene-C_{60} bisadduct by device optimization," *Advanced Materials*, vol. 22, no. 39, pp. 4355–4358, 2010.

[5] J.-L. Wu, F.-C. Chen, M.-K. Chuang, and K.-S. Tan, "Near-infrared laser-driven polymer photovoltaic devices and their biomedical applications," *Energy and Environmental Science*, vol. 4, no. 9, pp. 3374–3378, 2011.

[6] T.-Y. Chu, S. Alem, P. G. Verly et al., "Highly efficient polycarbazole-based organic photovoltaic devices," *Applied Physics Letters*, vol. 95, Article ID 063304, 2009.

[7] G. Namkoong, J. Kong, M. Samson, I. Hwang, and K. Lee, "Active layer thickness effect on the recombination process of PCDTBT:PC_{71}BM organic solar cells," *Organic Electronics*, vol. 14, no. 1, pp. 74–79, 2013.

[8] Z. He, C. Zhong, S. Su, M. Xu, H. Wu, and Y. Cao, "Enhanced power-conversion efficiency in polymer solar cells using an inverted device structure," *Nature Photonics*, vol. 6, no. 9, pp. 591–595, 2012.

[9] J. You, C. Chen, Z. Hong et al., "10.2% power conversion efficiency polymer tandem solar cells consisting of two identical sub-cells," *Advanced Materials*, vol. 25, no. 29, pp. 3973–3978, 2013.

[10] Y. Liang, Z. Xu, J. Xia et al., "For the bright future-bulk heterojunction polymer solar cells with power conversion efficiency of 7.4%," *Advanced Materials*, vol. 22, no. 20, pp. E135–E138, 2010.

[11] S. J. Lou, J. M. Szarko, T. Xu, L. Yu, T. J. Marks, and L. X. Chen, "Effects of additives on the morphology of solution phase aggregates formed by active layer components of high-efficiency organic solar cells," *Journal of the American Chemical Society*, vol. 133, no. 51, pp. 20661–20663, 2011.

[12] T. Salim, L. H. Wong, B. Bräuer et al., "Solvent additives and their effects on blend morphologies of bulk heterojunctions," *Journal of Materials Chemistry*, vol. 21, no. 2, pp. 242–250, 2011.

[13] F.-C. Chen, H.-C. Tseng, and C.-J. Ko, "Solvent mixtures for improving device efficiency of polymer photovoltaic devices," *Applied Physics Letters*, vol. 92, no. 10, Article ID 103316, 2008.

[14] A. J. Moulé and K. Meerholz, "Controlling morphology in polymer-fullerene mixtures," *Advanced Materials*, vol. 20, no. 2, pp. 240–245, 2008.

[15] K. K. H. Chan, S. W. Tsang, H. K. H. Lee, F. So, and S. K. So, "Charge injection and transport studies of poly(2,7-carbazole) copolymer PCDTBT and their relationship to solar cell performance," *Organic Electronics: Physics, Materials, Applications*, vol. 13, no. 5, pp. 850–855, 2012.

[16] J.-H. Huang, Y.-S. Hsiao, E. Richard et al., "The investigation of donor-acceptor compatibility in bulk-heterojunction polymer systems," *Applied Physics Letters*, vol. 103, Article ID 043304, 2013.

[17] B. J. Leever, C. A. Bailey, T. J. Marks, M. C. Hersam, and M. F. Durstock, "In situ characterization of lifetime and morphology in operating bulk heterojunction organic photovoltaic devices by impedance spectroscopy," *Advanced Energy Materials*, vol. 2, no. 1, pp. 120–128, 2012.